https://dx.doi.org/10.1016/j.ijbiomac.2023.125470

Guanidine-Containing Double-Network Silks with Enhanced Tensile and Antibacterial Property

*Chang Liu,[1] Xin Hu,[1] Xiang Zhou,[3] Yan Ma,[4] Polly H. M. Leung,[2] John H. Xin,[1] and Bin Fei [1]**

1 School of Fashion and Textiles, The Hong Kong Polytechnic University, Hong Kong, China

2 Department of Health Technology and Informatics, The Hong Kong Polytechnic University, Hong Kong, China

3 Department of Science, China Pharmaceutical University, Nanjing 211198, China

4 Jinzhou Central Hospital, Jinzhou, China

* Corresponding author: tcfeib@polyu.edu.hk

KEYWORDS: silk suture, double networks, antibacterial property.

ABSTRACT

The bacterial infection of surgical wounds results in prolonged hospitalization and even death of patients, calling for antibacterial function in modern suture products. To tackle this challenge, cationic guanidine-containing copolymer was synthesized, exhibiting antibacterial potency over 5 log reduction against both Gram-positive *S. aureus* and Gram-negative *E. coli*. Furthermore, we developed a double-network silk suture by integrating a guanidine-containing copolymer network into the silk fibroin network. This suture exhibited biocidal activity against *S. aureus* and *E. coli*, and superior strength compared to the commercial product in both dry and wet conditions. These results may bring general benefits to public health and medical equipment sustainability.

1. Introduction

Surgical site infections (SSIs) constitute the third most common hospital infection among patients and are also a significant cause of postoperative mortality [1]. Among various types of surgical implants, sutures are the most extensively used item, accounting for 57% of the global surgical equipment market. The application of antibacterial sutures would minimize the risk of SSIs [2, 3]. Furthermore, antibacterial modification has become a significant demand since the approval of triclosan-impregnated Polyglactin suture by the FDA in 2002. Natural non-absorbable silk sutures still have a place in modern surgical suture products due to their good biocompatibility and strength, which have been used as suture materials since ancient times [4]. However, silk sutures easily attract and hide microbes owing to their protein nature and construction structure, which brings adverse influence on their continuous

and widespread application. Their antibacterial functionalization becomes a necessary effort and remains a challenge.

So far, many different antibiotics such as amoxicillin trihydrate and levofloxacin hydrochloride have been incorporated in silk sutures [5-8]. However, the wide application of limited types of antibiotics has led to the emergence of more dangerous variants of bacteria with antibiotic resistance, such as methicillin-resistant *Staphylococcus aureus* (MRSA) and extended-spectrum β-lactamase-producing *Escherichia coli* (ESBL-EC) [9, 10]. More antibacterial mechanisms are in demand to enrich suture products and avoid the development of antibiotic-resistant bacteria. Heavy metal and metal oxide nanoparticles (e.g., Ag and ZnO) have also been deposited onto silk sutures for biomedical and antibacterial textile employment [11-13]. The various ways of disinfection of nanoparticles, such as cell wall disruption [14] and reactive oxygen species generation [15], set barriers for bacterial cells to develop resistance in comparison with antibiotics. However, the diffusion and accumulation of heavy metal nanoparticles in the environment raise concerns over their sustainability [16]. Thus, it is urgent and crucial to explore updated antiseptic agents for silk sutures.

Inherently antibacterial polymers and peptides have drawn much attention in antimicrobial therapeutics [17] and have been combined with silk fibers to achieve antibacterial function, such as chitosan [18], polyethyleneimine [19], 6mer-HNP1 antimicrobial peptide [20] and quaternary ammonium compound [21]. For instance, an antibacterial silk suture has been prepared by dip-coating with an antimicrobial peptide solution named 6mer-HNP1 [20], but the physical method of synthesis may cause the rapid leaching of the antimicrobial agent. In this regard, covalent-immobilized

antimicrobial polymers or peptides on silk sutures may provide long-term antibacterial ability [22]. In addition, natural organic compounds (e.g., arginine and agmatine) exhibited antimicrobial property, and guanidine groups are key to their antibacterial function [23]. For example, cationic guanidine-based nanosheets have been assembled into potential drug delivery vehicles for targeted therapies with low cytotoxicity and high transfection efficiency [24], killing bacteria by surface contact to disrupt cell membranes without the need of entering cells. Based on their safety, guanidine-containing polymers have been studied for hospital infection control and have proven effective in killing common bacteria as well as antibiotics-resistant clinically isolated bacteria [25]. Thus, guanidine is expected to be immobilized in silk sutures by chemical approaches to overcome bacterial antibiotic resistance and secure durable antibacterial property.

Besides bacterial attachment, the decrement in strength of silk sutures in wet state presents a potential risk for suture application in bio-tissues where high tension exists [26, 27]. Therefore, a new approach to manufacture long-term antibacterial silk sutures with enhanced strength is in demand. Inspired by research on dissolution system of silk fibroin and successful strategies for high-strength hydrogel fabrication [28-32], we propose to introduce double-network (DN) in the solid phase which has not been conducted before. DN structures are one of the most successful strategies for constructing hydrogel fibers to achieve enhanced strength and desired functionality [33-36], which is expected to be applied in silks to enhance their tensile and antibacterial property. Herein, we synthesized guanidine-containing copolymer and explored its antibacterial ability and mechanism. Furthermore, the guanidine-containing double-network silk suture with robust strength and biocidal property was fabricated by incorporating the guanidine-

containing network into the silk fibroin network, which may bring general benefits to public health and medical equipment sustainability.

2. Experimental section

2.1. Materials

Silk was supplied by Huasheng Industrial Co., China. Butyl acrylate (BA, ⩾99%, Sigma-Aldrich) and glycidyl methacrylate (GMA, 97%, Sigma-Aldrich) were distilled under reduced pressure with the addition of copper(I) bromide (98%, Sigma-Aldrich). 1,4-butanediol dimethacrylate (BDDMA, 95%, Sigma-Aldrich) was washed with alkaline aqueous solution and deionized water (DI water). Other chemicals were used without further purification including 2-hydroxy-4'-(2-hydroxyethoxy)-2-methylpropiophenone (Irgacure 2959, >98%, TCI), ethylenediamine (EDA, ⩾99%, Sigma-Aldrich), 1H-pyrazole-1-carboxamidine hydrochloride (HPC, 99%, Alfa Aesar), N,N-diisopropylethylamine (DIPEA, 99%, Aladdin), super dry tetrahydrofuran (THF, 99.9%, J&K), diethyl ether (⩾99.9%, VWR Chemicals), anhydrous calcium chloride ($CaCl_2$, VWR Chemicals), methanol (99.8%, Anaqua), ethanol (>95 %, Anaqua), N,N-dimethylformamide (DMF, 99.8%, Anaqua), chloroform-D ($CDCl_3$, 99.8 atom% D, Sigma-Aldrich) and deuterium oxide (D_2O, 99.8 atom% D, J&K Scientific).

2.2. Synthesis of guanidine-containing copolymer

BA-GMA copolymer was synthesized by free-radical polymerization. BA and GMA (molar ratio = 2:1) were mixed with photo-initiator Irgacure 2959 (1 w/v%), and irradiated under UV light (360–365 nm, 20 W) for 10 min. The prepared BA-GMA

copolymer (P(BA-GMA)) was then dissolved in super dry THF under stirring and precipitated twice in diethyl ether.

The procedure of further amination and guanidinylation were modified from previous literature [37]. The purified BA-GMA copolymer (0.1 g) was dissolved in super dry THF (30 mL), then EDA was added (10 mL) with the aim of complete ring-opening reaction of epoxide groups. The reaction mixture was stirred for 24 h, purified by dialysis (molecular weight (M.W.) cut off 3500) against DI water for 48 h, and then freeze-dried to yield BA-GMA-EDA copolymer (P(BA-GMA-EDA)).

The primary amines on BA-GMA-EDA copolymer were guanidinylated. The reaction was conducted in an aqueous solution of HPC (1.3 mmol) and DIPEA (1.3 mmol) for 24 h at room temperature. The modified copolymer was further purified by dialysis (M.W. cut off 3500) against DI water for 48 h, and then freeze-dried to yield guanidine-containing BA-GMA-EDA-G copolymer (P(BA-GMA-EDA-G)). The degree of substitution of guanidyl groups of the copolymer was estimated as 42%.

2.3. Fibroin filaments with guanidine-containing DN structures

Raw silk filament was winded on the roller and degummed by IR heating (AHIBA IR PRO, Datacolor) in sealed water at 120 °C for 90 min, then rinsed and dried at 60 °C overnight to obtain continuous fibroin filaments (FFs). Continuous FFs were winded onto Polytetrafluoroethylene (PTFE) framework and immersed in $CaCl_2$ (6 wt.%)–methanol (94 wt.%) solvent in a sealed bottle at 68 °C for 1 h. Then liquid exchange by immersion in monomers (BA and GMA, molar ratio = 2:1)–photo-initiator (Irgacure 2959, 1 w/v% of monomers)–crosslinker (BDDMA, 0.25 wt.% of monomers) precursor

solution for 10 min. The FFs were exposed to UV light for 10 min, and then immersed in super dry THF for purification for 12 h. The sample is defined as DN FF.

The procedure for further amination and guanidinylation of DN FFs was based on the synthesis of guanidine-containing copolymer with modifications [37]. EDA (10 mL) was added to super dry THF (30 mL), followed by DN FF (0.1 g). The reaction was run for 24 h in a shaker at room temperature with the aim of complete ring-opening reaction of epoxy groups. The resulting product was purified by immersing in DI water for 12 h and defined as EDA-DN FF.

The primary amines of the prepared EDA-DN FF were attempted for subsequent guanidinylation. The reaction was conducted in an aqueous solution with the presence of HPC (0.15 mmol) and DIPEA (0.15 mmol) to EDA-DN FF (1 mg) for 24 h incubation in a shaker at room temperature. The product was purified by rinsing with ethanol and DI water repeatedly, and the ultimate guanidine-containing double-network FF product was obtained and defined as G-DN FF.

2.4. Characterizations

The proton nuclear magnetic resonance (^{1}H NMR) spectra of P(BA-GMA) using $CDCl_3$ as solvent and P(BA-GMA-EDA) and P(BA-GMA-EDA-G) using D_2O as solvent were acquired on a 500 MHz NMR spectrometer (Jeol ECZ500R). The molecular weight of P(BA-GMA) was measured by the gel permeation chromatography (GPC, Waters 1515, USA) using DMF as the mobile phase and polystyrene as the calibration substance. P(BA-GMA-EDA) and P(BA-GMA-EDA-G) were dispersed in THF and dropped onto clean silicon slices, dried in the air and then coated with gold

by sputtering for SEM observation (VEGA3, Tescan). The particle size distribution and zeta potential of P(BA-GMA-EDA-G) in aqueous dispersion were determined using a zetasizer instrument (Malvern). Attenuated total reflection Fourier-transform infrared spectra (ATR-FTIR) were acquired in the region of 4000–650 cm^{-1} with 64 scans at 4 cm^{-1} resolution by a spectrometer (Spectrum 100, PerkinElmer). Silk suture was prepared by twister (400 tpm) and fixed by hot steam (90 s). The commercial silk suture (dyed virgin silk W870, Ethicon®, U.S. Pharmacopeia (USP) 8-0, twisted construction) was purchased from Johnson & Johnson Co., LTD. The morphologies were observed under an optical light microscope (M165C, Lecia) and a microscope with polarizers (DM2700M, Leica). The tension tests including the straight-pull and surgeon's knot-pull were performed using an Instron 5944 with a 10 N load cell and a gauge length of 20 mm at a speed of 10 mm/min, where dry samples were standard-conditioned at 25 ± 2 °C and relative humidity of 65 ± 5% for 24 h while wet samples were soaked in DI water for 12 h before the test.

2.5. Antibacterial properties

Bacterial count: Gram-positive bacteria *Staphylococcus aureus* (*S. aureus*, ATCC 6538) and Gram-negative bacteria *Escherichia coli* (*E. coli*, ATCC 25922) were used to investigate the antibacterial property of guanidine-containing copolymer and fiber. The microorganisms were cultured in 10 ml Luria–Bertani (LB) broth at 37 °C for 18 h to obtain a bacterial suspension of approximately 2–5 × 10^9 CFU/mL. This bacterial suspension was diluted 10^4 and 10^7 times with phosphate-buffered saline (PBS, pH=7.4) as working bacterial suspension for guanidine-containing copolymer and fiber, respectively. P(BA-GMA-EDA-G) with different concentrations and bacterial suspensions were incubated and shaken for 18 h at 37 °C. The bacteria incubated

without the addition of P(BA-GMA-EDA-G) served as the control group. After that, the suspensions were serial diluted to 1/1000, and 100 μL of the diluted suspensions were then plated (in triplicate) on the solid LB agar plates, followed by incubation for 24 h at 37 °C. Additionally, bacterial suspensions with 0.02 g/mL of original FF or G-DN FF samples were incubated and shaken for 5 h at 37 °C. After that, 100 μL of the suspensions were plated (in triplicate) on the solid LB agar plates, followed by incubation for 24 h at 37 °C. The antibacterial properties were evaluated as log reduction of the colony-forming units per milliliter (CFU/mL).

Zeta potential measurement: The procedure was from previous literature with modification [38]. Bacterial suspensions in PBS (10^9 CFU/mL, 100 μL) were incubated alone or with P(BA-GMA-EDA-G) (1 mg/mL) at 37 °C for 3 min. After that, bacterial cells were collected by centrifugation and washed with PBS twice, followed by being suspended in DI water (1 mL). The obtained samples were kept on ice for zeta potential measurement.

Field emission scanning electron microscope (FESEM) characterization: Bacterial cells were harvested from the control and P(BA-GMA-EDA-G) treated groups by centrifugation and washed with PBS twice. The morphology of bacteria was fixed in glutaraldehyde (GA, 2.5%) aqueous solution at room temperature for 4 h, which was centrifuged to remove supernatant and washed with PBS twice. Subsequently, the bacteria were dehydrated with gradient ethanol (30%, 50%, 70%, 80%, 90%, and 100% for 30 min, respectively). Ultimately, the specimens were dropped onto clean silicon slices, dried in the air and then coated with gold by sputtering for FESEM observation

(Tescan MAIA3). The fixation and dehydration procedures were also performed for the original FF and G-DN FF samples tested for bacterial count on LB agar plates.

Live/Dead bacterial staining assay: The bacterial suspensions of control and P(BA-GMA-EDA-G) treated groups were washed with PBS twice and re-dispersed in PBS. Subsequently, the suspensions were stained with SYTO 9 and propidium iodide (PI) in darkness for 20 min. Then, the bacterial cells were harvested by centrifuge and washed three times with PBS and resuspended in PBS. The suspensions were then dropped onto the glass slide and covered with a coverslip. The observation of samples was executed by confocal laser scanning microscopy (CLSM, Leica SPE microscope) using a 488 nm laser.

2.6. Statistical analysis

All test data were expressed as mean ± standard deviation (S.D.). Statistical significance was analyzed by one-way analysis of variance (ANOVA) with post hoc Tukey testing. The *p* value less than 0.05 was considered to be statistically significant.

3. Results and discussion

The synthetic route for a series of copolymers is shown in Figure 1a. P(BA-GMA) was prepared via photo-polymerization; then primary amine groups were added by the ring-opening reaction of epoxy groups with EDA, forming P(BA-GMA-EDA). The obtained primary amines reacted with guanidylation reagent to yield guanidine-containing P(BA-GMA-EDA-G). Correspondingly, as illustrated in Figure 1b, silk suture (i.e., FF suture) with DN structures (DN FF suture) was formed through swelling process ($CaCl_2$–methanol solvent) and liquid exchange (BA and GMA precursor

solution). This additional network provided reactive functional groups to FF suture for following amination (forming EDA-DN FF suture) and guanidinylation (forming G-DN FF suture) reactions. The guanidinylation manufacturing process was operated in convenient and facile condition with aqueous solution at room temperature. The cationic guanidine-containing copolymer (P(BA-GMA-EDA-G)) and suture (G-DN FF suture) showed antibacterial property, being potential candidates for biomedicine and suture application.

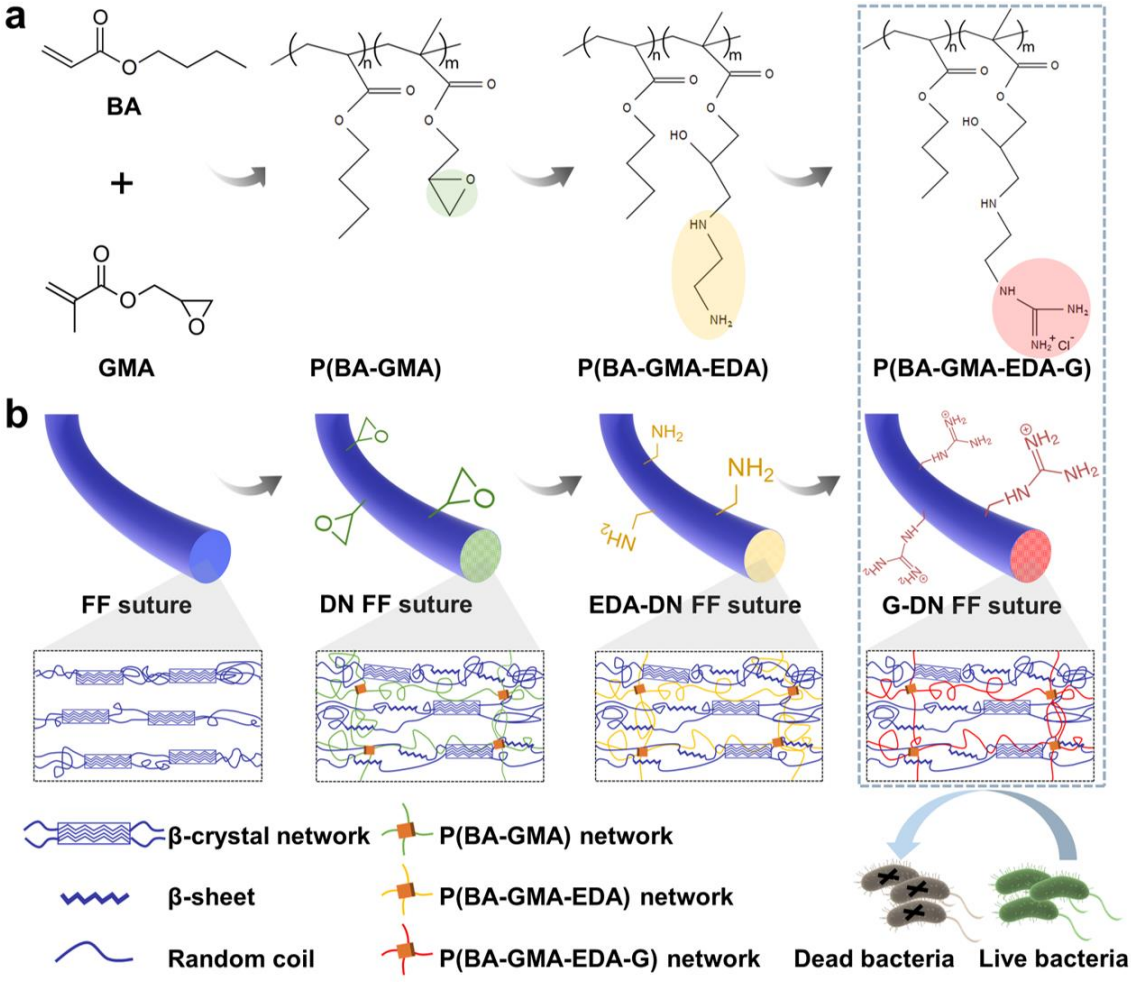

Figure 1. (a) Synthetic diagram of guanidine-containing copolymer and (b) the manufacturing of toughened antimicrobial silk suture with guanidine-containing double networks, exhibiting biocidal property.

^{1}H NMR spectroscopy was utilized to reveal the chemical structure of the obtained copolymers (Figure 2a). In Figure 2ai, the peaks at 2.64 ppm, 2.83 ppm and 3.22 ppm were ascribed to the epoxy groups on the side chain of P(BA-GMA) [39, 40]. The peaks at 3.81 ppm, 3.99 ppm and 4.28 ppm were contributed to methylene protons adjacent to the ester groups [41]. The molar ratio of GMA and BA in P(BA-GMA) was calculated as 1:1.1 by peak integration based on the indicative peaks of GMA (2.64 and 2.83 ppm) and BA (1.37 ppm), which was higher than their initial feeding molar ratio 1:2 due to higher reactivity ratio of GMA in comparison with BA [42]. After ring-opening reaction of epoxy groups with EDA, the peaks at 2.57–2.94 ppm were assigned to methylene groups linked to the amino group in P(BA-GMA-EDA) as shown in Figure 2aii [37]. After guanidinylation on the primary amines in P(BA-GMA-EDA), the peak at 3.32 ppm appeared and was attributed to methylene groups in proximity to guanidine groups as shown in Figure 2aiii [37]. Hence, ^{1}H NMR results demonstrated the successful synthesis of guanidine-containing P(BA-GMA-EDA-G). The successful synthesis of P(BA-GMA-EDA-G) was also confirmed by FTIR spectra (Figure S1). A new peak at 1540 cm^{-1} was observed in the spectrum of P(BA-GMA-EDA) compared to P(BA-GMA), which was attributed to C−N stretching vibration resulting from the increased presence of primary amine due to EDA treatment [37, 43]. As compared to P(BA-GMA-EDA), a new peak at 1662 cm^{-1} appeared in the spectrum of P(BA-GMA-EDA-G), corresponding to the stretching vibration of C=N. This demonstrates the introduction of guanidine into the P(BA-GMA-EDA) [44, 45]. Additionally, the molecular weight of P(BA-GMA) was calculated as 4828 g/mol (Figure S2). The morphologies of P(BA-GMA-EDA) and P(BA-GMA-EDA-G) were shown in Figure S3. Furthermore, the size distribution of P(BA-GMA-EDA-G) particles self-assembled in H_2O was measured by

dynamic light scattering to be narrow at around 232 ± 20 nm (Figure 2b). In Figure 2c, P(BA-GMA-EDA-G) particles had a positive zeta potential (35.6 ± 2.9 mV), showing a large number of cationic charges on the guanidine-containing copolymer particles, which may play a key role in bactericidal actions.

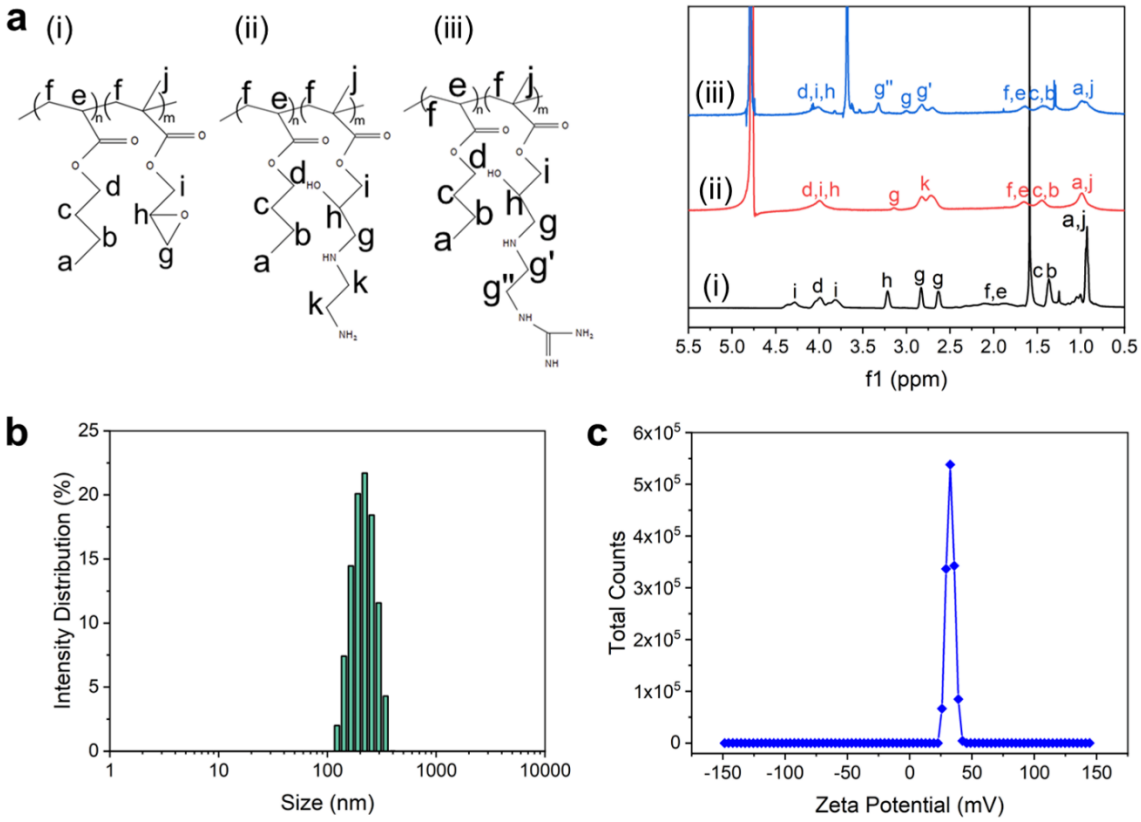

Figure 2. (a) ^{1}H NMR spectra of copolymers including (i) P(BA-GMA) in $CDCl_3$, (ii) P(BA-GMA-EDA) and (iii) P(BA-GMA-EDA-G) in D_2O. (b) The size distribution and (c) zeta potential of P(BA-GMA-EDA-G) particles in H_2O.

The antibacterial activities of P(BA-GMA-EDA-G) against Gram-positive *S. aureus* and Gram-negative *E. coli* are shown in Figure 3a, b. P(BA-GMA-EDA-G) at a concentration of 15.6 μg/mL offered 0.52 log (70.01%) reduction and 0.60 log (74.88%) reduction of *S. aureus* and *E. coli*, respectively, exhibiting bactericidal ability over these

two bacterial strains. The higher concentration of 31.3–125 μg/mL of P(BA-GMA-EDA-G) showed over 5.20 log (99.999%) reduction and 5.07 log (99.999%) reduction in *S. aureus* and *E. coli*. Therefore, the minimum bactericidal concentrations (MBCs) of P(BA-GMA-EDA-G) against *S. aureus* and *E. coli* were 31.3 μg/mL, which refers to the lowest concentration that leads to a 3 log reduction (99.9% killing) [46]. The representative LB agar plates in Figure 3c reflected the inactivation of *S. aureus* and *E. coli* from the concentration of 31.3 μg/mL, demonstrating the remarkable antibacterial ability of P(BA-GMA-EDA-G). Moreover, MBC values of P(BA-GMA-EDA-G) against *S. aureus* and *E. coli* were much lower in comparison with other literatures [47-52] (Figure 3d, e and Table 1).

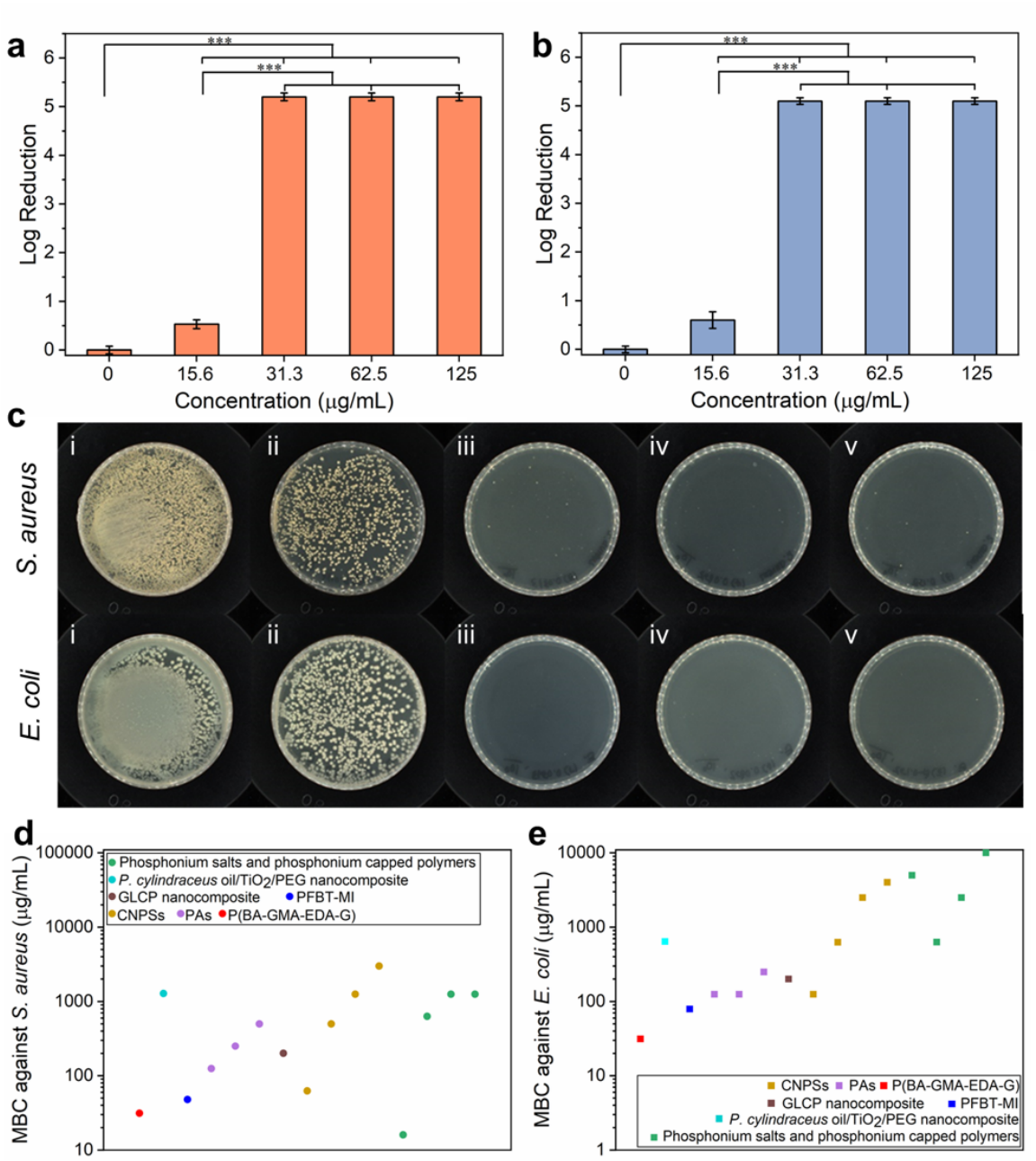

Figure 3. Log reduction of (a) *S. aureus* and (b) *E. coli* treated with different concentrations of P(BA-GMA-EDA-G) (***$p < 0.001$). (c) Representative LB agar plates of *S. aureus* and *E. coli* colonies treated with P(BA-GMA-EDA-G) with different concentrations: (i) 0 (control), (ii) 15.6, (iii) 31.3, (iv) 62.5 and (v) 125 μg/mL. (d, e) Comparison of MBC values of synthesized polymers and polymeric nanocomposites against *S. aureus* and *E. coli*. [47-52]

Table 1. Comparison of MBC values of synthesized polymers and polymeric nanocomposites against *S. aureus* and *E. coli*.

Material	Bacteria	MBC (μg/mL)	Treatment condition	*Reference*
Phosphonium salts and phosphonium capped polymers	*S. aureus*	16–1250	RT, 4h	*47*
	E. coli	630–10000		
Plectranthus cylindraceus (*P. cylindraceus*) oil/TiO_2/PEG nanocomposite	*S. aureus*	1280	37 °C, 24 h	*48*
	E. coli	640		
Graphene oxide/lanthanum coordination polymer (GLCP nanocomposite)	*S. aureus*	200	37 °C, 24 h	*49*
	E. coli	200		
Cationic conjugated polyelectrolyte (PFBT-MI)	*S. aureus*	47.7	37 °C, 12 h	*50*
	E. coli	79		
Cationic nanopolystyrenes (CNPSs)	*S. aureus*	62.5–3000	37 °C, 20 h	*51*
	E. coli	125–4000		
Aromatic polyamides (PAs)	*S. aureus*	125–500	37 °C, 24 h	*52*
	E. coli	125–250		
P(BA-GMA-EDA-G)	*S. aureus*	31.3	37 °C, 18 h	*This work*
	E. coli	31.3		

In order to gain insight into the interaction between P(BA-GMA-EDA-G) and bacteria, we employed zeta potential measurement, FESEM characterization and CLSM characterization. The surface zeta potentials of bacteria before and after treatment with P(BA-GMA-EDA-G) were measured to illustrate possible interactions between bacteria and P(BA-GMA-EDA-G) [19, 53, 54]. As shown in Figure 4a, the zeta potentials of *S. aureus* and *E. coli* were -27.9 mV and -34.2 mV, respectively, indicating the negative charge on the bacterial surface owing to carboxyl and phosphate groups of teichoic acids in Gram-positive bacteria and phosphate groups of phospholipids and

lipopolysaccharides in Gram-negative bacteria [55]. Regarding the bacteria treated with P(BA-GMA-EDA-G), there was an obvious shift in their surface zeta potentials to 8.9 mV and 24.5 mV for *S. aureus* and *E. coli*, respectively. Such shift was attributed to the association of cationic guanidine-containing copolymer and negative charge on the bacterial surface via electrostatic interaction, which is consistent with previous literature [56]. Here, a more obvious shift of zeta potentials occurred in *E. coli* than that of *S. aureus*, because Gram-positive bacteria like *S. aureus* have thicker cell walls and stronger bacterial self-defense than Gram-negative bacteria like *E. coli* [19]. The zeta potential results were also in accordance with bacterial count assay results presented in Figure 3a, b. P(BA-GMA-EDA-G) at a concentration of 15.6 μg/mL exhibited higher bactericidal ability against *E. coli* (74.88% reduction) than *S. aureus* (70.01% reduction). From the FESEM images (Figure 4b, c), the morphologies of untreated bacteria (control) showed original and intact spherical (*S. aureus*) in Figure 4bi, biii and rod-like (*E. coli*) morphologies in Figure 4ci, ciii, respectively. In contrast, the bacteria treated with P(BA-GMA-EDA-G) exhibited obvious cellular deformation as well as partial or complete membrane lysis (Figure 4bii, iv and Figure 4cii, iv) [57, 58]. The FESEM images are in well agreement with zeta potential results. Furthermore, the live/dead bacterial staining assay was performed and observed by CLSM using a 488 nm laser via the dual fluorescent stains of SYTO 9 and PI [56, 59]. SYTO 9 stained both live and dead bacterial cells in green fluorescence, while PI only penetrated through the ruptured bacterial membranes of the dead bacterial cells and stained in red fluorescence [22]. In Figure 4d (i, iii) and 4e (i, iii), *S. aureus* and *E. coli* displayed green fluorescence and negligible red fluorescence, demonstrating bacterial cells were viable and cell membranes mainly remained intact in control groups [22]. However, *S. aureus* and *E. coli* after treatment by P(BA-GMA-EDA-G) exhibited both green and red fluorescence in

Figure 4d (ii, iv) and 4e (ii, iv). The cells in green were almost exclusively in red, suggesting the cell membranes were damaged by P(BA-GMA-EDA-G) [22], which agrees with FESEM images. In short, the cationic guanidine groups of P(BA-GMA-EDA-G) could quickly bind with anionic groups in cell membranes or walls, leading to osmotic damage and cell membrane disruption, followed by intercellular leakage and cell lysis. Therefore, P(BA-GMA-EDA-G) displayed potent antimicrobial properties against *S. aureus* and *E. coli*.

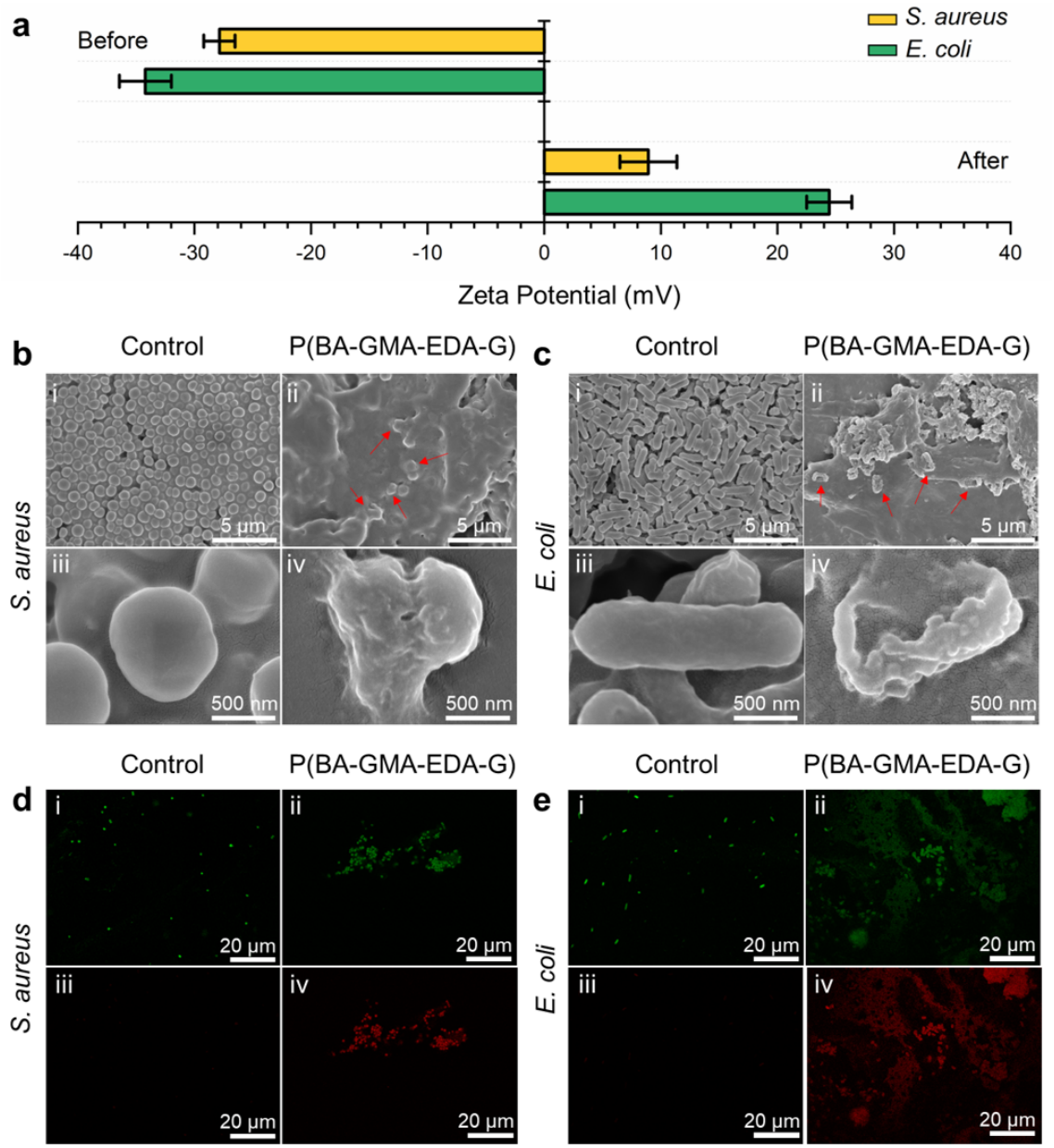

Figure 4. (a) Zeta potentials of *S. aureus* and *E. coli* before and after treated with P(BA-GMA-EDA-G). FESEM images of (b) *S. aureus* and (c) *E. coli* treated with PBS (i, iii) and P(BA-GMA-EDA-G) (ii, iv), respectively. CLSM images of (d) *S. aureus* and (e) *E. coli* treated with PBS (i, iii) and P(BA-GMA-EDA-G) (ii, iv), respectively, stained by SYTO 9 (green fluorescence, for alive/dead cells)/PI (red fluorescence, only for dead cells).

Based on the powerful antibacterial guanidine-containing copolymer, guanidine-containing DN FF (G-DN FF) was fabricated to obtain silk sutures with antimicrobial activity and enhanced tensile properties. The chemical change and secondary structure of FF samples were investigated by FTIR. The FTIR spectra in Figure 5a presented the common features of peptide skeleta of amide I (1618 cm^{-1}, C=O stretching vibration), amide II (1512 cm^{-1}, mainly N−H bending vibration), and amide III (1228 cm^{-1}, mainly C−N stretching vibration) of FFs [60, 61]. Compared with the spectrum of original FF, G-DN FF was characterized by the bands at 1720 cm^{-1}, in the region of 1689–1630 cm^{-1}, 1578 cm^{-1}, and 1539 cm^{-1}, which existed in the spectrum of P(BA-GMA-EDA-G). The peak at 1720 cm^{-1} was assigned to ester C=O stretching vibration [62], and the peaks at 1578 cm^{-1} and 1539 cm^{-1} were attributed to N−H distortion vibration and C−N stretching vibration due to the increase of primary amine by EDA treatment [37, 43]. In addition, the peaks at 1662 cm^{-1} (C=N stretching vibration), 1645 cm^{-1} (N−H bending vibration) and 1628 cm^{-1} (C−N stretching vibration) in the spectrum of G-DN FF were noticed, confirming the guanidyl groups have been bound to the DN FF [44, 45]. The FTIR spectrum of EDA-DN FF is shown in Figure S1. The antimicrobial properties against *S. aureus* and *E. coli* of original FF and G-DN FF are shown in Figure 5b. The original FF had no antibacterial property, while G-DN FF offered more than 2.61 log (99.76%)

reduction and 2.30 log (99.50%) reduction against *S. aureus* and *E. coli*, indicating that the introduced guanidine-containing network endowed FF with antibacterial activities by means of contact bacteria through electrostatic attraction, causing cell membrane disruption. Representative LB agar plates in Figure 5c illustrated the total deactivation of *S. aureus* and *E. coli* by the G-DN FF in sharp contrast to the original FF. FESEM images also showed the cell membrane deformation and disintegration of bacteria adhered to G-DN FF as shown in Figure 5d.

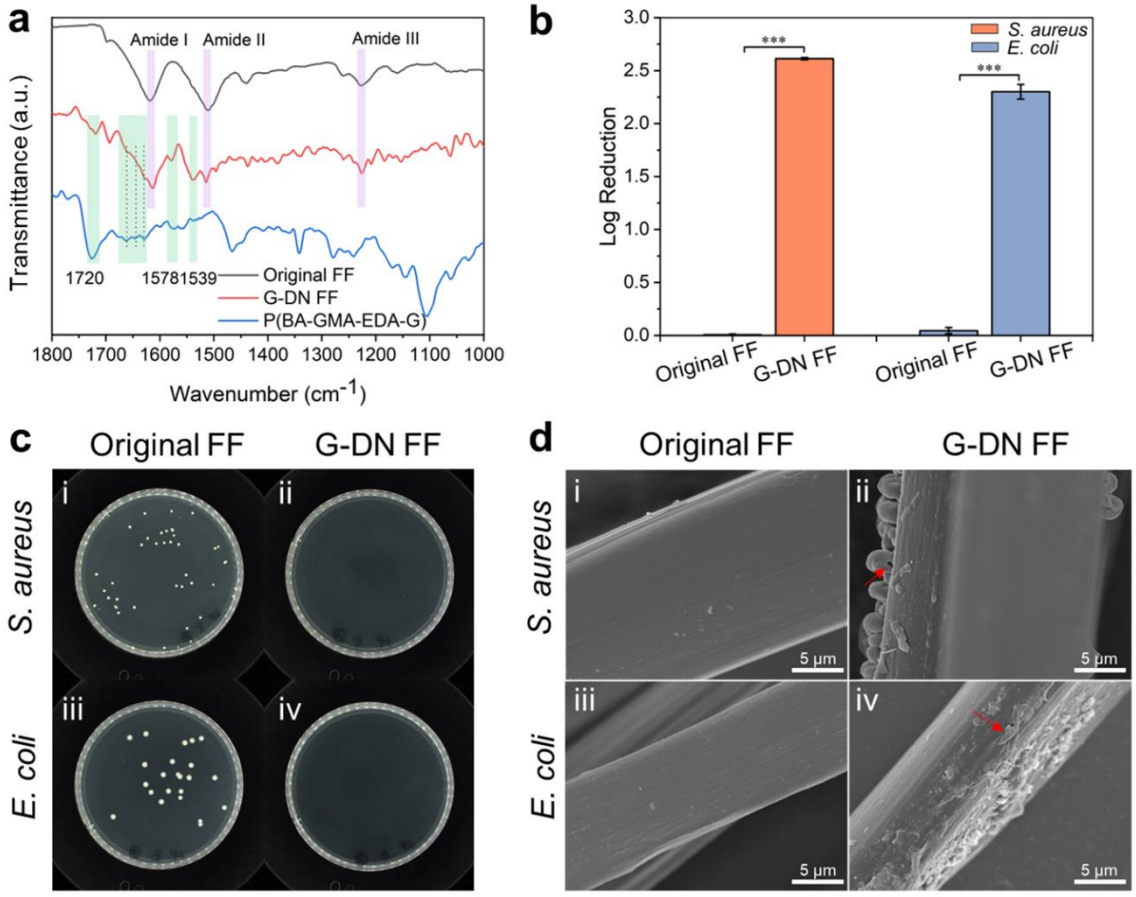

Figure 5. (a) FTIR spectra of original FF, G-DN FF and P(BA-GMA-EDA-G). (b) Log reduction of *S. aureus* and *E. coli* treated with original FF and G-DN FF (***$p < 0.001$). (c) Representative LB agar plates of *S. aureus* and *E. coli* colonies treated with original

FF (i, iii) and G-DN FF (ii, iv). (d) FESEM images of original FF (i, iii) and G-DN FF (ii, iv) against *S. aureus* and *E. coli*.

The breaking force is a crucial factor for suture applications. Undoubtedly, silk is chosen as surgical suture material due to its biocompatibility, sufficient strength and good handling characteristics [63]. However, the strength of silk decreases in the wet tissue environment, because of its water absorption tendency and unstable amorphous phase [27, 64]. The lower wet strength of silk suture is a concern to cause surgical failure, which can be resolved in this work. The morphologies of G-DN FF suture are shown in Figure 6a, involving straight/knot state (i) and birefringence characteristic (ii, iii), which were similar with commercial silk suture (Figure 6b). In the straight-pull test (Figure 6c and Table 2), the breaking force of G-DN FF suture and commercial SF suture were 1.20 N and 0.93 N, respectively. In the wet state, G-DN FF suture and commercial SF suture exhibited a 21% and 33% decrease in the maximum breaking force. In the knot-pull test, the limit on average knot-pull breaking force for U.S. Pharmacopeia (USP) 8-0 non-absorbable sutures are 0.59 N (Class I, e.g., silk suture) and 0.39 N (class II, e.g., virgin silk suture) according to USP monographs [65]. The representative knot-pull force−strain curves of G-DN FF suture and commercial silk suture are shown in Figure 6d. Their knot-pull breaking forces were 0.88 N and 0.60 N (see Table 2), respectively, which were lower than the straight-pull breaking force. This might be caused by the stress concentration on knot position during stretching. In addition, wetting resulted in obvious reductions in knot-pull breaking force of G-DN FF suture (0.69 N, with a reduction of 22%) and commercial silk suture (0.45 N, with a reduction of 25%). The wet knot-pull breaking force of G-DN FF suture was comparable to dry values of commercial silk suture and USP standard, despite suffering

from weakening in the wet state. Hence, G-DN FF suture was successfully manufactured and showed biocidal property against Gram-positive (*S. aureus*) and Gram-negative (*E. coli*) strains. Furthermore, the strength of G-DN FF suture was superior to that of the commercial product in dry and wet conditions, making it a promising candidate in modern surgical suture fields.

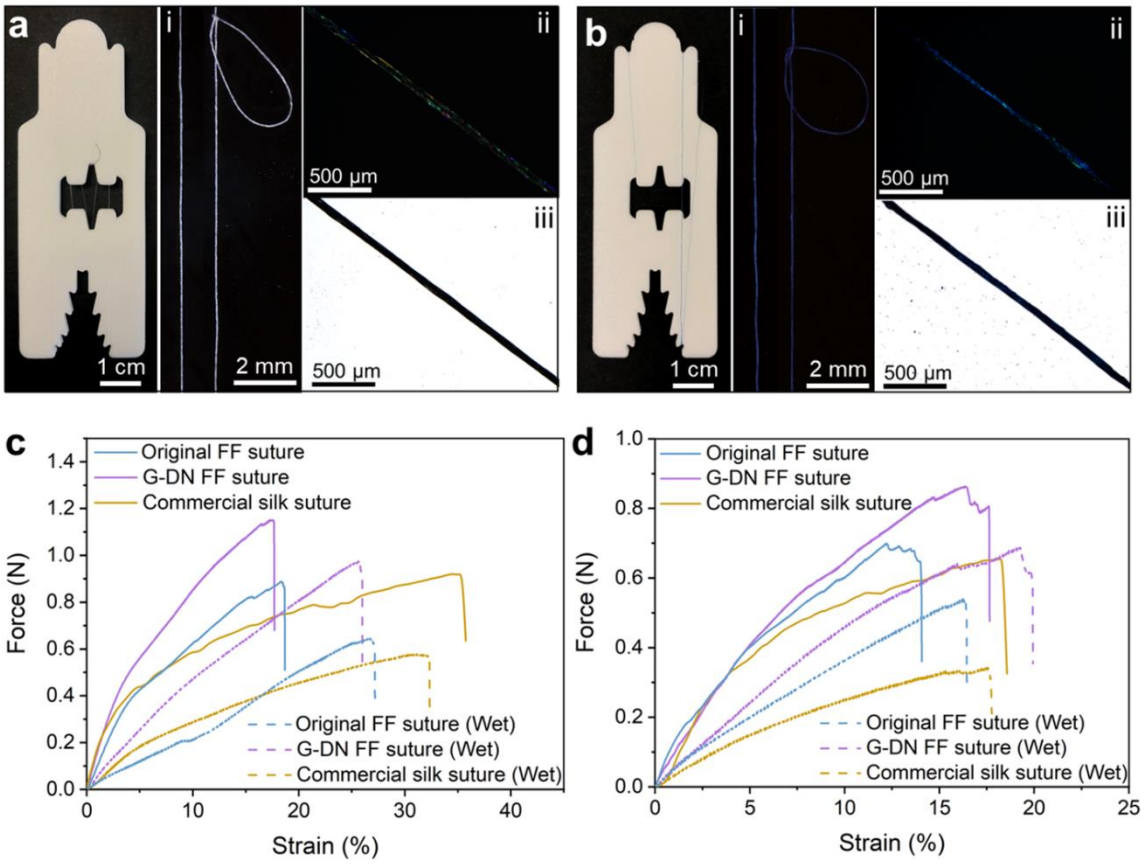

Figure 6. The photograph of (a) G-DN FF suture and (b) commercial silk suture with different morphologies including microscopic images in (i) straight and knot state and polarized microscopic images under crossed polarizers (ii) and without polarizers (iii). The representative (c) straight-pull and (d) knot-pull force−strain curves of original FF suture, G-DN FF suture and commercial silk suture in both dry and wet conditions.

Table 2. Tensile properties of original FF suture, G-DN FF suture and commercial silk suture (n=3).

Test type	Suture type	Breaking force (N)	Elongation at break (%)
Straight-pull test	Original FF suture	0.92 ± 0.03 b	18.9 ± 0.4 b
	G-DN FF suture	1.20 ± 0.18 a	17.7 ± 3.7 b
	Commercial silk suture	0.93 ± 0.02 b	30.9 ± 5.6 a
Straight-pull test (wet)	Original FF suture	0.65 ± 0.01 b	26.1 ± 3.2 a
	G-DN FF suture	0.95 ± 0.03 a	29.7 ± 6.0 a
	Commercial silk suture	0.62 ± 0.04 b	32.5 ± 2.3 a
Knot-pull test	Original FF suture	0.67 ± 0.08 b	14.5 ± 3.0 a
	G-DN FF suture	0.88 ± 0.09 a	15.0 ± 2.8 a
	Commercial silk suture	0.60 ± 0.07 b	16.2 ± 4.5 a
Knot-pull test (wet)	Original FF suture	0.53 ± 0.02 a	19.8 ± 3.1 a
	G-DN FF suture	0.69 ± 0.11 a	24.0 ± 5.4 a
	Commercial silk suture	0.45 ± 0.10 b	19.1 ± 3.8 a

Means ± SD with different letters in the same column differed significantly ($P< 0.05$).

4. Conclusions

In conclusion, a copolymer containing epoxide groups was synthesized by free-radical polymerization, and was further grafted with primary amines via ring-opening reaction of epoxide groups with ethylenediamine. Guanidine-containing copolymer was further synthesized by primary amine guanidinylation. Antibacterial efficiency of guanidine-containing copolymer reached over 5 log reduction against both Gram-positive *S. aureus* and Gram-negative *E. coli*. The antibacterial mechanism was attributed to the integration of cationic guanidine groups of copolymers with anionic groups at surfaces of bacterial cells, resulting in osmotic damage and cell membrane

disruption, followed by intercellular leakage and cell lysis, as revealed by zeta potential, FESEM and CLSM characterization. Moreover, guanidine-containing polymer network was incorporated in silk fibroin network to form guanidine-containing DN silk suture. The resultant guanidine-containing DN silk suture exhibited antibacterial property against both *S. aureus* and *E. coli* and strength superior to the commercial product in dry and wet states, serving as a promising candidate for surgical suture application. This photo synthesis of bactericidal double network approach can be extended to other solid substrates, such as membranes and coatings.

AUTHOR INFORMATION

Corresponding Author

*Bin Fei − School of Fashion and Textiles, The Hong Kong Polytechnic University, Hong Kong, China; Email: tcfeib@polyu.edu.hk

Author Contributions

C.L. and B.F. conceptualized the project; C.L. designed and performed research; C.L. and X.H. performed experiments; C.L. performed analyzed data; Polly H.M.L. provided antibacterial platform and guidance; B.F. provided supervision throughout the study; C.L. wrote the original draft; C.L., X.H., X.Z., Y.M., Polly H.M.L., John H. X. and B.F. reviewed and edited the manuscript. All authors have read and agreed to the published version of the manuscript.

Notes

The authors declare no competing financial interest.

ACKNOWLEDGMENT

This work was supported by the General Research Fund PolyU152156/17E of the Hong Kong Research Grant Council and a matching fund G-YBRF from Hong Kong Polytechnic University.

REFERENCES

1. Magill, S. S.; Edwards, J. R.; Bamberg, W.; Beldavs, Z. G.; Dumyati, G.; Kainer, M. A.; Lynfield, R.; Maloney, M.; McAllister-Hollod, L.; Nadle, J.; Ray, S. M.; Thompson, D. L.; Wilson, L. E.; Fridkin, S. K., Multistate Point- Prevalence Survey of Health Care- Associated Infections. *N. Engl. J. Med.* **2014,** *370* (13), 1198-1208.

2. Tummalapalli, M.; Anjum, S.; Kumari, S.; Gupta, B., Antimicrobial Surgical Sutures: Recent Developments and Strategies. *Polym. Rev.* **2016,** *56* (4), 607-630.

3. Ming, X.; Rothenburger, S.; Yang, D., In vitro antibacterial efficacy of MONOCRYL plus antibacterial suture (Poliglecaprone 25 with triclosan). *Surg. Infect.* **2007,** *8* (2), 201-208.

4. Thilagavathi, G.; Viju, S., Silk as a suture material. In *Advances in Silk Science and Technology*, 2015; pp 219-232.

5. Chen, X.; Hou, D.; Wang, L.; Zhang, Q.; Zou, J.; Sun, G., Antibacterial Surgical Silk Sutures Using a High-Performance Slow-Release Carrier Coating System. *ACS Appl. Mater. Interfaces* **2015,** *7* (40), 22394-22403.

6. Choudhury, A. J.; Gogoi, D.; Chutia, J.; Kandimalla, R.; Kalita, S.; Kotoky, J.; Chaudhari, Y. B.; Khan, M. R.; Kalita, K., Controlled antibiotic-releasing Antheraea

assama silk fibroin suture for infection prevention and fast wound healing. *Surgery* **2016,** *159* (2), 539-547.

7. Wu, D. Q.; Cui, H. C.; Zhu, J.; Qin, X. H.; Xie, T., Novel amino acid based nanogel conjugated suture for antibacterial application. *J. Mater. Chem. B* **2016,** *4* (15), 2606-2613.

8. Chen, X.; Hou, D.; Tang, X.; Wang, L., Quantitative physical and handling characteristics of novel antibacterial braided silk suture materials. *J. Mech. Behav. Biomed. Mater.* **2015,** *50*, 160-170.

9. Ventola, C. L., The antibiotic resistance crisis: part 1: causes and threats. *Pharmacy and therapeutics* **2015,** *40* (4), 277-283.

10. Baym, M.; Lieberman, T. D.; Kelsic, E. D.; Chait, R.; Gross, R.; Yelin, I.; Kishony, R., Spatiotemporal microbial evolution on antibiotic landscapes. *Science* **2016,** *353* (6304), 1147-1151.

11. De Simone, S.; Gallo, A. L.; Paladini, F.; Sannino, A.; Pollini, M., Development of silver nano-coatings on silk sutures as a novel approach against surgical infections. *J. Mater. Sci. Mater. Med.* **2014,** *25* (9), 2205-2214.

12. Lu, Z.; Meng, M.; Jiang, Y.; Xie, J., UV-assisted in situ synthesis of silver nanoparticles on silk fibers for antibacterial applications. *Colloids Surf., A* **2014,** *447*, 1-7.

13. Shubha, P.; Gowda, M. L.; Namratha, K.; Shyamsunder, S.; Manjunatha, H. B.; Byrappa, K., Ex-situ fabrication of ZnO nanoparticles coated silk fiber for surgical applications. *Mater. Chem. Phys.* **2019,** *231*, 21-26.

14. Abo-zeid, Y.; Williams, G. R., The potential anti-infective applications of metal oxide nanoparticles: A systematic review. *Wiley Interdiscip. Rev.: Nanomed. Nanobiotechnol.* **2020,** *12* (2), e1592.

15. Dizaj, S. M.; Lotfipour, F.; Barzegar-Jalali, M.; Zarrintan, M. H.; Adibkia, K., Antimicrobial activity of the metals and metal oxide nanoparticles. *Mater. Sci. Eng., C* **2014,** *44*, 278-284.

16. Giovanni, M.; Tay, C. Y.; Setyawati, M. I.; Xie, J.; Ong, C. N.; Fan, R.; Yue, J.; Zhang, L.; Leong, D. T., Toxicity profiling of water contextual zinc oxide, silver, and titanium dioxide nanoparticles in human oral and gastrointestinal cell systems. *Environ. Toxicol.* **2015,** *30* (12), 1459-1469.

17. Ghalei, S.; Handa, H., A Review on Antibacterial Silk Fibroin-based Biomaterials: Current State and Prospects. *Mater. Today Chem.* **2022,** *23*, 100673.

18. Hosseini, M.; Montazer, M.; Damerchely, R., Enhancing dye-ability and antibacterial features of silk through pre-treatment with chitosan. *J. Eng. Fibers Fabr.* **2013,** *8* (3), 102-111.

19. Wang, F.; Yan, B.; Li, Z.; Wang, P.; Zhou, M.; Yu, Y.; Yuan, J.; Cui, L.; Wang, Q., Rapid Antibacterial Effects of Silk Fabric Constructed through Enzymatic Grafting of Modified PEI and AgNP Deposition. *ACS Appl. Mater. Interfaces* **2021,** *13* (28), 33505-33515.

20. Franco, A. R.; Fernandes, E. M.; Rodrigues, M. T.; Rodrigues, F. J.; Gomes, M. E.; Leonor, I. B.; Kaplan, D. L.; Reis, R. L., Antimicrobial coating of spider silk to prevent bacterial attachment on silk surgical sutures. *Acta Biomater.* **2019,** *99*, 236-246.

21. Meghil, M. M.; Rueggeberg, F.; El-Awady, A.; Miles, B.; Tay, F.; Pashley, D.; Cutler, C. W., Novel coating of surgical suture confers antimicrobial activity against Porphyromonas gingivalis and Enterococcus faecalis. *J. Periodontol.* **2015,** *86* (6), 788-794.

22. Han, H.; Zhu, J.; Wu, D. Q.; Li, F. X.; Wang, X. L.; Yu, J. Y.; Qin, X. H., Inherent Guanidine Nanogels with Durable Antibacterial and Bacterially Antiadhesive Properties. *Adv. Funct. Mater.* **2019,** *29* (12), 1806594.

23. Kim, S.-H.; Semenya, D.; Castagnolo, D., Antimicrobial drugs bearing guanidine moieties: A review. *Eur. J. Med. Chem.* **2021,** *216*, 113293.

24. Treat, N. J.; Smith, D.; Teng, C.; Flores, J. D.; Abel, B. A.; York, A. W.; Huang, F.; McCormick, C. L., Guanidine-Containing Methacrylamide (Co)polymers via aRAFT: Toward a Cell Penetrating Peptide Mimic. *ACS Macro Lett.* **2012,** *1* (1), 100-104.

25. Zhou, Z.; Wei, D.; Guan, Y.; Zheng, A.; Zhong, J.-J., Extensive in vitro activity of guanidine hydrochloride polymer analogs against antibiotics-resistant clinically isolated strains. *Mater. Sci. Eng., C* **2011,** *31* (8), 1836-1843.

26. Perez-Rigueiro, J.; Viney, C.; Llorca, J.; Elices, M., Mechanical properties of silkworm silk in liquid media. *Polymer* **2000,** *41* (23), 8433-8439.

27. Liu, C.; Hua, J.; Ng, P. F.; Wang, Y.; Fei, B.; Shao, Z., Bioinspired Photo-Cross-Linking of Stretched Solid Silks for Enhanced Strength. *ACS Biomater. Sci. Eng.* **2022,** *8* (2), 484-492.

28. Shen, T.; Wang, T.; Cheng, G.; Huang, L.; Chen, L.; Wu, D., Dissolution behavior of silk fibroin in a low concentration CaCl2-methanol solvent: From morphology to nanostructure. *Int. J. Biol. Macromol.* **2018,** *113*, 458-463.

29. Ng, P. F.; Lee, K. I.; Meng, S.; Zhang, J.; Wang, Y.; Fei, B., Wet Spinning of Silk Fibroin-Based Core–Sheath Fibers. *ACS Biomater. Sci. Eng.* **2019,** *5* (6), 3119-3130.

30. Ng, P. F.; Hua, J.; Liu, C.; Wang, Y.; Yin, R.; Fei, B., Solar Energy Storage Silks via Coaxial Wet Spinning. *ACS Mater. Lett.* **2020,** *2* (7), 801-807.

31. Liu, C.; Hua, J.; Ng, P. F.; Fei, B., Photochemistry of bioinspired dityrosine crosslinking. *J. Mater. Sci. Technol.* **2021,** *63*, 182-191.

32. Hua, J.; Ng, P. F.; Fei, B., High-strength hydrogels: Microstructure design, characterization and applications. *J. Polym. Sci., Part B: Polym. Phys.* **2018,** *56* (19), 1325-1335.

33. Hua, J.; Liu, C.; Ng, P. F.; Fei, B., Bacterial cellulose reinforced double-network hydrogels for shape memory strand. *Carbohydr. Polym.* **2021,** *259*, 117737.

34. Hua, J.; Liu, C.; Fei, B.; Liu, Z., Self-Healable and Super-Tough Double-Network Hydrogel Fibers from Dynamic Acylhydrazone Bonding and Supramolecular Interactions. *Gels* **2022,** *8* (2), 101.

35. Lu, X.; Chan, C. Y.; Lee, K. I.; Ng, P. F.; Fei, B.; Xin, J. H.; Fu, J., Super-tough and thermo-healable hydrogel - promising for shape-memory absorbent fiber. *J. Mater. Chem. B* **2014,** *2* (43), 7631-7638.

36. Wu, F.; Chen, L.; Wang, Y.; Fei, B., Tough and stretchy double-network hydrogels based on in situ interpenetration of polyacrylamide and physically cross-linked polyurethane. *J. Mater. Sci.* **2019,** *54* (18), 12131-12144.

37. Guo, P.; Gu, W.; Chen, Q.; Lu, H.; Han, X.; Li, W.; Gao, H., Dual functionalized amino poly(glycerol methacrylate) with guanidine and Schiff-base linked imidazole for enhanced gene transfection and minimized cytotoxicity. *J. Mater. Chem. B* **2015,** *3* (34), 6911-6918.

38. Yan, S.; Chen, S.; Gou, X.; Yang, J.; An, J.; Jin, X.; Yang, Y. W.; Chen, L.; Gao, H., Biodegradable Supramolecular Materials Based on Cationic Polyaspartamides and Pillar[5]arene for Targeting Gram-Positive Bacteria and Mitigating Antimicrobial Resistance. *Adv. Funct. Mater.* **2019,** *29* (38), 1904683.

39. Wang, L.; Yang, Y.-W.; Zhu, M.; Qiu, G.; Wu, G.; Gao, H., β-Cyclodextrin-conjugated amino poly(glycerol methacrylate)s for efficient insulin delivery. *RSC Adv.* **2014,** *4* (13), 6478-6485.

40. Tsarevsky, N. V.; Bencherif, S. A.; Matyjaszewski, K., Graft copolymers by a combination of ATRP and two different consecutive click reactions. *Macromolecules* **2007,** *40* (13), 4439-4445.

41. Jones, M.-C.; Tewari, P.; Blei, C.; Hales, K.; Pochan, D. J.; Leroux, J.-C., Self-assembled nanocages for hydrophilic guest molecules. *J. Am. Chem. Soc.* **2006,** *128* (45), 14599-14605.

42. Bakhshi, H.; Zohuriaan-Mehr, M.; Bouhendi, H.; Kabiri, K., Spectral and chemical determination of copolymer composition of poly (butyl acrylate-co-glycidyl methacrylate) from emulsion polymerization. *Polym. Test.* **2009,** *28* (7), 730-736.

43. Segal, L.; Eggerton, F., Infrared spectra of ethylenediamine and the dimethylethylenediamines. *Appl. Spectrosc.* **1961,** *15* (4), 116-117.

44. Jermakowicz-Bartkowiak, D.; Kolarz, B.; Serwin, A., Sorption of precious metals from acid solutions by functionalised vinylbenzyl chloride–acrylonitryle–divinylbenzene copolymers bearing amino and guanidine ligands. *React. Funct. Polym.* **2005,** *65* (1-2), 135-142.

45. Ran, J.; Wang, N.; You, X.; Wu, C.; Li, Q.; Gong, M.; Xu, T., Guanidylated hollow fiber membranes based on brominated poly (2,6-dimethyl-1,4-phenylene oxide) (BPPO) for gold sorption from acid solutions. *J. Hazard. Mater.* **2012,** *241-242*, 63-72.

46. Wang, X.; Liu, C.; Meng, D.; Sun, J.; Fei, B.; Li, H.; Gu, X.; Zhang, S., Surface integration of polyelectrolyte and zeolitic imidazolate framework-67 for multifunctional poly (lactic acid) non-woven fabrics. *Appl. Surf. Sci.* **2021,** *569*, 151039.

47. Hisey, B.; Ragogna, P. J.; Gillies, E. R., Phosphonium-Functionalized Polymer Micelles with Intrinsic Antibacterial Activity. *Biomacromolecules* **2017,** *18* (3), 914-923.

48. Amina, M.; Al Musayeib, N. M.; Alarfaj, N. A.; El-Tohamy, M. F.; Al-Hamoud, G. A., Antibacterial and Anticancer Potentials of Presynthesized Photosensitive Plectranthus cylindraceus Oil/TiO2/Polyethylene Glycol Polymeric Bionanocomposite. *Bioinorg. Chem. Appl.* **2021,** *2021*, 5562206.

49. Wang, J.; Shan, Z.; Tan, X.; Li, X.; Jiang, Z.; Qin, J., Preparation of graphene oxide (GO)/lanthanum coordination polymers for enhancement of bactericidal activity. *J. Mater. Chem. B* **2021,** *9* (2), 366-372.

50. Zehra, N.; Dutta, D.; Malik, A. H.; Ghosh, S. S.; Iyer, P. K., Fluorescence Resonance Energy Transfer-Based Wash-Free Bacterial Imaging and Antibacterial Application Using a Cationic Conjugated Polyelectrolyte. *ACS Appl. Mater. Interfaces* **2018,** *10* (33), 27603-27611.48.

51. Wen, Q.; Xu, L.; Xiao, X.; Wang, Z., Preparation, characterization, and antibacterial activity of cationic nanopolystyrenes. *J. Appl. Polym. Sci.* **2019,** *137* (8), 48405.

52. Dinari, M.; Fardmanesh, K.; Maleki, M. H.; Asadi, P., Synthesis, characterization and antimicrobial properties of new L-cysteine based chiral aromatic polyamides. *Polym. Bull.* **2022,** *79* (12), 11103-11117.

53. Halder, S.; Yadav, K. K.; Sarkar, R.; Mukherjee, S.; Saha, P.; Haldar, S.; Karmakar, S.; Sen, T., Alteration of Zeta potential and membrane permeability in bacteria: a study with cationic agents. *Springerplus* **2015,** *4*, 672.

54. Chen, L.; Bai, H.; Xu, J. F.; Wang, S.; Zhang, X., Supramolecular Porphyrin Photosensitizers: Controllable Disguise and Photoinduced Activation of Antibacterial Behavior. *ACS Appl. Mater. Interfaces* **2017,** *9* (16), 13950-13957.

55. Feng, P.; Luo, Y.; Ke, C.; Qiu, H.; Wang, W.; Zhu, Y.; Hou, R.; Xu, L.; Wu, S., Chitosan-Based Functional Materials for Skin Wound Repair: Mechanisms and Applications. *Front. Bioeng. Biotechnol.* **2021,** *9*, 650598.

56. Guo, S.; Huang, Q.; Chen, Y.; Wei, J.; Zheng, J.; Wang, L.; Wang, Y.; Wang, R., Synthesis and Bioactivity of Guanidinium-Functionalized Pillar[5]arene as a Biofilm Disruptor. *Angew. Chem. Int. Ed.* **2021,** *60* (2), 618-623.

57. Cheung, Y. H.; Ma, K.; van Leeuwen, H. C.; Wasson, M. C.; Wang, X.; Idrees, K. B.; Gong, W.; Cao, R.; Mahle, J. J.; Islamoglu, T.; Peterson, G. W.; de Koning, M. C.; Xin, J. H.; Farha, O. K., Immobilized Regenerable Active Chlorine within a Zirconium-Based MOF Textile Composite to Eliminate Biological and Chemical Threats. *J. Am. Chem. Soc.* **2021,** *143* (40), 16777-16785.

58. Ma, L.; Zhang, Z.; Li, J.; Yang, X.; Fei, B.; Leung, P. H. M.; Tao, X., A New Antimicrobial Agent: Poly (3-hydroxybutyric acid) Oligomer. *Macromol. Biosci.* **2019,** *19* (5), e1800432.

59. Stiefel, P.; Schmidt-Emrich, S.; Maniura-Weber, K.; Ren, Q., Critical aspects of using bacterial cell viability assays with the fluorophores SYTO9 and propidium iodide. *BMC Microbiol.* **2015,** *15*, 36.

60. Barth, A., The infrared absorption of amino acid side chains. *Prog. Biophys. Mol. Biol.* **2000,** *74* (3-5), 141-173.

61. Boulet-Audet, M.; Vollrath, F.; Holland, C., Identification and classification of silks using infrared spectroscopy. *J. Exp. Biol.* **2015,** *218* (19), 3138-3149.

62. Wu, X.; Li, J.; Wang, J.; Cao, L., Poly(butyl acrylate) gel prepared in supercritical CO2: an efficient recyclable oil-absorbent. *Int. J. Ind. Chem.* **2020,** *11* (2), 91-99.

63. Koh, L.-D.; Cheng, Y.; Teng, C.-P.; Khin, Y.-W.; Loh, X.-J.; Tee, S.-Y.; Low, M.; Ye, E.; Yu, H.-D.; Zhang, Y.-W., Structures, mechanical properties and applications of silk fibroin materials. *Prog. Polym. Sci.* **2015,** *46*, 86-110.

64. Lee, K. I.; Wang, X.; Guo, X.; Yung, K.-F.; Fei, B., Highly water-absorbing silk yarn with interpenetrating network via in situ polymerization. *Int. J. Biol. Macromol.* **2017,** *95*, 826-832.

65. United States Pharmacopeia (2022). USP Monographs, Nonabsorbable Surgical Suture. USP-NF. Rockville, MD: United States Pharmacopeia. https://doi.usp.org/USPNF/USPNF_M80200_04_01.html